Task-oriented Learnable Diffusion Timesteps for Universal Few-shot Learning of Dense Tasks

Changgyoon Oh*, Jongoh Jeong*, Jegyeong Cho*, Kuk-Jin Yoon

Visual Intelligence Lab., KAIST
{changgyoon,jeong2,j2k0618,kjyoon}@kaist.ac.kr

Abstract. Denoising diffusion probabilistic models have brought tremendous advances in generative tasks, achieving state-of-the-art performance thus far. Current diffusion model-based applications exploit the power of learned visual representations from multistep forward-backward Markovian processes for single-task prediction tasks by attaching a task-specific decoder. However, the heuristic selection of diffusion timestep features still heavily relies on empirical intuition, often leading to sub-optimal performance biased towards certain tasks. To alleviate this constraint, we investigate the significance of versatile diffusion timestep features by adaptively selecting timesteps best suited for the few-shot dense prediction task, evaluated on an arbitrary unseen task. To this end, we propose two modules: Task-aware Timestep Selection (TTS) to select ideal diffusion timesteps based on timestep-wise losses and similarity scores, and Timestep Feature Consolidation (TFC) to consolidate the selected timestep features to improve the dense predictive performance in a few-shot setting. Accompanied by our parameter-efficient fine-tuning adapter, our framework effectively achieves superiority in dense prediction performance given only a few support queries. We empirically validate our learnable timestep consolidation method on the large-scale challenging *Taskonomy* dataset for dense prediction, particularly for practical *universal* and *few-shot* learning scenarios.

Keywords: Diffusion Models, Diffusion Timestep Selection, Universal Few-shot Dense Prediction

1 Introduction

In recent years, diffusion models [1–7] have been a trending topic in the computer vision community, particularly spearheading the image generation task. Their success is largely attributed to the ability to generate diverse images in high quality and resolution by sequentially attending to rich texture and semantic information in an iterative Markovian process. With the emergence and burst of diffusion model-based applications in various other tasks ranging from generative modeling tasks [8–12] such as image super-resolution to discriminative tasks [**?**, **?**, 13–17] such as semantic segmentation, researchers have geared their focus toward approaches that are resource efficient and fully leverage diffusion model features to the maximum potential. In this regard, several works

have considered the use of various timesteps from Denoising Diffusion Probabilistic Models (DDPM) [1] with analysis of the distinctive characteristics of the denoising features in the early and late timesteps [1, 18]. Specifically, due to the successive denoising process, earlier timesteps attend to global structures (*e.g.,* general semantic structure), while later timesteps concentrate more on local structures (*e.g.,* high-frequency details). Baranchuk *et al*. [19] has further expanded these findings to semantic segmentation, one of the fundamental computer vision tasks, achieving phenomenal results by leveraging intermediate activations from the U-Net backbone network [20]. Succeeding their work, Diffusion Hyperfeatures [21] employ aggregated intermediate activations at multiple empirically predefined timesteps for the semantic correspondence task. Nevertheless, all of these works are limited in scalability and universal applicability because of the heuristic selection timestep features for a specific task.

In this light, we throw key essential questions for best leveraging diffusion models for dense prediction tasks: (1) Do certain diffusion timestep features contribute more to any task(s) in particular? and (2) Are there diffusion timestep features that can be generalizable to multiple tasks in a practical setting? With ongoing debate about which timestep(s) to select, which timestep features are mutually beneficial for multiple tasks, and how to use them effectively in a unified learning framework, we aim to address this challenge by closely examining the correlation between timestep features and a target task with appropriate selection of timestep features. We specifically analyze their relationship for dense prediction tasks in a *universal few-shot* learning setup, whereby *universality* and *few-shot* applicability are each verified by evaluating on an *unseen, arbitrary* target task, and fine-tuning with a small, limited number of support data samples.

To this end, we employ a pre-trained Latent Diffusion Model (LDM), which is known to compress semantic information impressively in a latent vector without substantial distortion in the image quality, in a challenging dense prediction task. To be specific, we take a bold step forward to examine the role of diffusion timesteps in relation to a given task in a few-shot setting, a scenario in which only a few support image-label pairs are available. As opposed to prior approaches, we propose two modules to assist in composing a solid set of timestep features to aid the few-shot learner in dense prediction without the need for manually defined timesteps. In our Task-aware Timestep Selection (TTS) module, we repeatedly search for a new timestep feature that is ideal for the particular task, while in Timestep Feature Consolidation (TFC) module, we merge the selected ones before predicting the label. Through our approach, we aim to address and alleviate the current problem of inevitably selecting diffusion timestep features either empirically or heuristically due to the lack of prior knowledge, and unleash the relationship between these features and target tasks via in-depth analyses. We crucially note that ours stands as a pioneering work on searching for ideal diffusion timesteps to extend and generalize to multiple tasks and is applicable to other works that require off-the-shelf pre-trained diffusion models.

In summary, we present our contributions as follows:

- We, for the first time in the relevant literature, present a task-aware timestep selection module to search for ideal timesteps containing task-specific context. Subsequently, we also propose a timestep feature consolidation module to effectively fuse task-specific timestep features with support label features for few-shot learning.
- We demonstrate that our proposed method, further guided by parameter-efficient fine-tuning, is effective and robust in few-shot dense prediction against unseen, arbitrary tasks as validated on the large-scale challenging Taskonomy-*Tiny* dataset.
- To showcase the effectiveness of our adaptive timestep consolidation approach, we extensively discuss and compare quantitative and qualitative performance with those using heuristic timesteps as in previous works.

2 Related Work

2.1 Diffusion Probabilistic Models

Denoising diffusion probabilistic models (DDPMs) [1, 3–7, 22, 23] are a family of generative models that has emerged recently, significantly surpassing the performance of image generation tasks. DDPMs perform forward diffusion process to model data distribution and generate new samples by reversing the same process. At an earlier time of appearance, their progress was hampered by significantly large memory and time resource requirements. Dhariwal *et al.* [24] then introduced an improved form of a DDPM called Guided Diffusion, beating GANs [25] by a noticeable margin. In addition, Latent Diffusion Models (LDM) [4] introduced a latent variable into the diffusion process to capture complex dependencies in the data, leading to more expressive generative models. Stable Diffusion [4] is a type of LDM that can be conditioned with visual or textual representations from models pre-trained with large-scale datasets (*e.g.,* CLIP [26]) or condition-free for image generation.

Numerous diffusion model-based works have demonstrated the representative power of DDPMs as high-performing representation learners for single [27, 28] and multiple tasks [5, 19, 29]. With a large portion of works grounded on text-to-image aligned models [30, 31], many employ such text-to-image models without explicit text input, *i.e.,* with blank text input [29–31], due to the lack of image-aligned text prompts in the existing datasets.

2.2 Diffusion Timestep-aware Learning

Since the birth of DDPMs, numerous studies have brought diffusion models to use in their respective task and field. In general, we can categorize their uses based on single and multiple timesteps.

Single timestep. VPD [30] proposes a dense prediction architecture using the first timestep feature from text-to-image diffusion models. Li *et al.* [32] empirically choose the best timestep, $t = 5$, among 1000 timesteps for open-vocabulary object segmentation. In contrast to manually fixing one timestep, both DiffusionNeRF [33] and DreamFusion [34] heuristically select a timestep to fully distill

the knowledge to the NeRF model for realistic 2D rendering. Nonetheless, it is inevitable to spend time- and memory-intensive resource costs to acquire consistently promising performance with such heuristic use of timestep features. Our approach, in contrast, devises a systematic approach to sampling adequate timesteps to secure outperforming performance across multiple target tasks.

Multiple timesteps. There have been efforts to use several or a group of timestep features to arrive at ideal timesteps for a target task. For instance, AutoDiffusion [6] accelerates the sampling process by searching through space to select an optimal timestep sequence by using the evolutionary algorithm. Their search process relies on a metric to estimate performance at a certain timestep. They specifically adopt the FID metric, a key criterion for assessing image generation, which is their target task. On the contrary, our method estimates the adequacy of the timestep by task-agnostic measure, namely timestep-wise loss, as well as timestep feature similarity metrics for general applicability, *i.e.,* dense prediction task.

Wang *et al*. [35] propose a hybrid quality score to detect semantics-related timesteps to guide other image manipulator, and Baranchuk *et al*. [19] and Diffusion Hyperfeatures [21] are subsequent works for semantic segmentation and semantic correspondence, respectively, which leverage aggregated diffusion features from the reverse process. ODISE [36] also concatenates multiple pre-defined timesteps for open-vocabulary panoptic segmentation. A major inherent drawback in these works is the heuristic selection of diffusion timesteps for the task-specific purpose. We, in contrast, explore a learnable and more task-generalized approach to select the most appropriate timesteps for multiple tasks altogether.

2.3 Universal Few-shot Dense Prediction

Few-shot learning methods for dense prediction focus on specific target tasks, and most of them are only targeted on the tasks that require categorical labels such as object detection [37–40], semantic segmentation [41–44] and instance segmentation [45,46]. Some works utilize correlation between support and query sets [47, 48] or mappings from features to segmentation masks like DenseGP [49]. However, these methods are still limited to a curated set of tasks with prior task-specific knowledge or assumptions, thus not suitable in practical scenarios that require application to unseen, arbitrary tasks. In this regard, Visual Token Matching [50] (VTM) presents the *first* unified framework for *universal* few-shot learning of dense tasks, following the episodic meta-learning protocol [51] to adapt to unseen arbitrary dense prediction tasks.

2.4 Parameter-efficient Fine-tuning

Parameter-efficient Fine-tuning (PEFT) is an emerging field of research with the burst of large pre-trained models put to diverse applications, including large language models (LLMs) [52,53] and large multimodal models (LMMs) [54,55]. Current PEFT methods can be categorized into three branches. Adapter-based

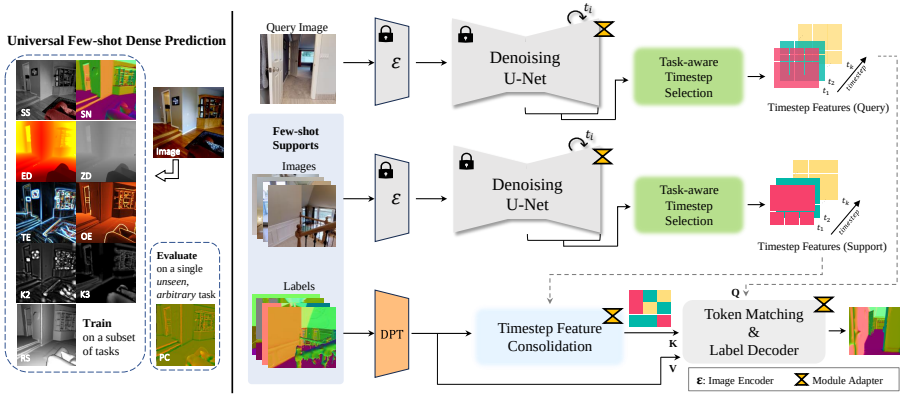

Fig. 1: Overall training pipeline of our few-shot learner optimized with diffusion timestep features. Our learning framework operates based on the selected timestep features from the denoising diffusion model pre-trained on a large-scale dataset. As opposed to previous works that rely on heuristic and intuitive selection of diffusion timesteps for a specific task, we leverage the visual representation power from the pre-trained latent diffusion model to search, select, and consolidate multiple timestep features to universally predict dense tasks given a few-shot supports.

approaches [56, 57] add a set of trainable parameters to the frozen backbone either in serial, parallel, or both. Prompt-based approaches attach extra soft token vectors to the input to train on fine-tuning. Finally, low-rank reparameterization adaptation, or LoRA [58–63], decomposes the weight matrices into approximate low-rank matrices to fine-tune alongside the frozen backbone weights. Recent PEFT approaches have branched out from LoRA to apply to low-rank adjustment [60, 62], weight update [64, 65], multi-task fine-tuning [66, 67]. Recent studies [68–70] also verified the generalizability of LoRA when fine-tuning diffusion models across tasks.

3 Proposed Method

We tackle the problem of universal few-shot dense prediction, whereby we opt to select ideal diffusion timesteps for an unseen, arbitrary target task. Our approach involves training the network on the training images, fine-tuning it on a few-shot (10) support images (representing less than 0.004% of the dataset), and testing it on a single arbitrary task that remains *unseen* during training. We particularly focus on a challenging yet performant setting in which we train on tasks belonging to four folds of relevant tasks and fine-tune on a single *unseen* task in the remaining fold as in [50].

3.1 Method Overview

We visually outline our overall training and inference pipelines in Fig. 1. To assess the effectiveness of our diffusion timestep selection and consolidation strategies, we incorporate a pre-trained LDM [4] as the image encoder and DPT [71] as

Algorithm 1 Task-aware Timestep Selection (TTS)

Require: N-block pre-trained diffusion decoder $\mathcal{D}$;
k initial diffusion timesteps $\mathcal{T}_0 \leftarrow \{t_1, t_2, \cdots, t_k\}$;
Timestep features $\mathcal{F}_{\mathcal{T}_0} \leftarrow D(\mathcal{T}_0)$;
Max. # of allowed timestep searches N_{iter};
Similarity threshold τ_{sim}
Ensure: $t_i \neq t_j,\ \forall t_i, t_j \in \mathcal{T}_0$
Compute sum of timestep-wise loss $\sum \mathcal{L}_{\mathcal{T}_0}$ ▷ Eq. 2
Remove $t_r \in \mathcal{T}_0$ with the largest timestep-wise loss ▷ $\mathcal{T}_0 \leftarrow \mathcal{T}_0 \setminus \{t_r\}$
for $i \leftarrow 1$ **to** N_{iter} **do**
    Randomly sample a new timestep $t_{\text{new}} \sim U(1, \sqcup_{\max})$
    Acquire timestep features $\mathcal{F}_{\mathcal{T}_i} \leftarrow D(\mathcal{T}_i)$
    Acquire new timestep feature $f_{t_{\text{new}}} \leftarrow D(t_{\text{new}})$
    Compute similarity score $\mathcal{S}_i \leftarrow \text{Sim}\big(f_{t_{\text{new}}}, \mathcal{F}_{\mathcal{T}_i}\big)$
    if $\mathcal{S}_i < \tau_{\text{sim}},\ \forall t \in \mathcal{T}_i$ **then**
        Forward pass model and compute loss $\mathcal{L}_{\text{prev}} \leftarrow \sum \mathcal{L}_{\mathcal{T}_i}$
        Remove $t_r \in \mathcal{T}_i$ with largest timestep-wise loss
        Compute loss with updated timestep set $\mathcal{L}_{\text{new}} \leftarrow \sum \mathcal{L}_{\{\mathcal{T}_i \cup t_{\text{new}}\}}$
        if $\mathcal{L}_{\text{new}} < \mathcal{L}_{\text{prev}}$ **then**
            Update timestep features $\mathcal{F}_{\mathcal{T}_i} \leftarrow \mathcal{F}_{\mathcal{T}_i} \cup f_{t_{\text{new}}}$
            break
        end if
    end if
end for
return $\mathcal{F}_{\mathcal{T}_i}$

the support label encoder to seamlessly evaluate our method into the existing pipeline for universal few-shot dense prediction.

Preliminaries. Visual Token Matching [50] (VTM) is the first work for the universal learning of few-shot (10 support images) dense prediction tasks. VTM uses the episodic meta-learning protocol [51] to learn the adaptability to the unseen arbitrary dense prediction tasks with a single unified network. It finds the correlation between the query image and support images and labels to exploit the hints for unseen target tasks. To obtain the correlation, it uses the attention mask of query image $X^q = \{x_j^q\}_{j \leq M} \in \mathbb{R}^{h \times w \times 3}$, support image $X^s = \{x_k^s\}_{k \leq M \times N} \in \mathbb{R}^{h \times w \times 3}$ and support labels $Y^s = \{y_j^s\}_{k \leq M \times N} \in \mathbb{R}^{h \times w \times C}$ to predict query label $Y^q = \{y_j^q\}_{j \leq M} \in \mathbb{R}^{h \times w \times C}$ where C is the number of channels of the target task. The total framework can be represented as follows:

$$g(y_j^q) = \sum_{k \leq M \times N} \sigma(f(x_j^q), f(x_k^s)) g(y_k^s) \tag{1}$$

where the grid size of images and labels are $M = h \times w$, x_j is the j-th patch, N is the number of the shot and σ represents the matching network (token matching network) such as patch-wise attention mechanisms while $f(\cdot)$ and $g(\cdot)$ denote the image and label encoder, ImageNet-22K [72] pre-trained BEiT-B model [73] and DPT [71] architecture from scratch, respectively. Through the

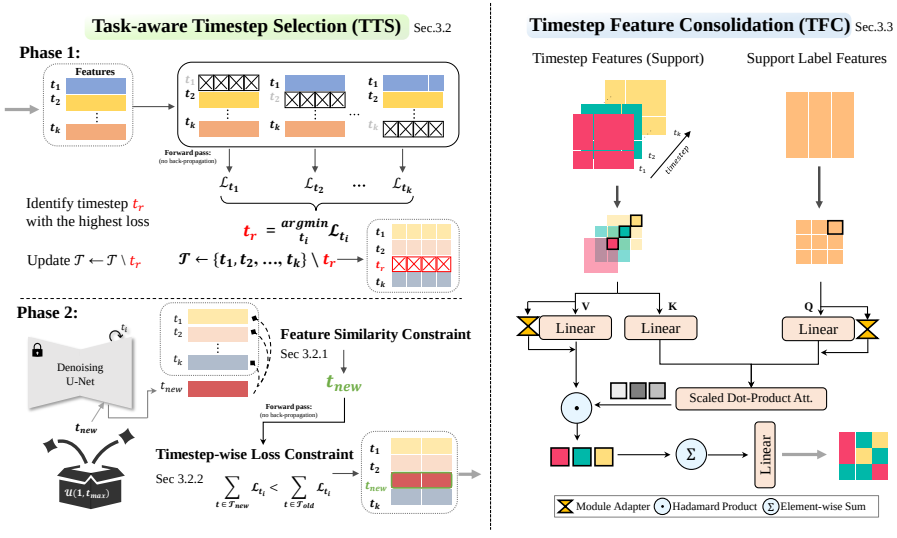

Fig. 2: Detailed description of our proposed TTS module and TFC module. Our TTS module takes as input k diffusion timestep features and searches for a new timestep at which its corresponding feature contains more semantically meaningful information than the previous. We first identify the least meaningful timestep feature based on the sum of task losses based on Leave-One-Out procedure, and then selects a new timestep feature under the feature similarity constraint and the resulting task loss. We repeat the selection process for N_{iter} steps until we find a new timestep feature. TFC module matches the image timestep features and label features to examine the effectiveness of each timestep, following the general cross attention mechanism.

matching network, image features of query sets and support sets are matched on the label embedding space which enables to exploit the similarity of images $\sigma(f(x^q), f(x^s))$ for predicting the label features of query sets from given support labels. In the end of training, obtained query label features $g(y^q)$ are decoded into the real label y^q by employing the decoder $h \approx g^{-1}$. After training, it is fine-tuned on the unseen arbitrary dense prediction tasks with small trainable parameters like the other parameter-efficient methods [56, 74–78].

Detailed Architecture. Adopting the state-of-the-art architecture for universal few-shot dense prediction, we follow the traces of [50] to modify to fit to our diffusion model-based few-shot learning setting with dynamic semantics.

From the original VTM architecture comprising a pre-trained image encoder f, a label encoder g, a matching network and a label decoder h, we distinguish the following modifications in our framework to integrate diffusion timestep features. First, we change the ViT-based image encoder to a Stable Diffusion [4] v1.4 model pre-trained on LAION-5B dataset [79] with small additional projection layers. In addition, our training flow differs in that we pass noisy images to the diffusion model in order to extract diffusion timestep features from the pre-traind U-Net blocks, which we then forward pass to several convolutional layers

to aggregate. We then attain timestep features, $f(x) \in \mathbb{R}^{(M\times N\times T)\times d}$, where T is the number of diffusion timesteps for the timestep matching module and d is the dimension of the each vector. The label encoder g and label decoder h are based on the DPT [71] architecture, similar to the VTM trained from scratch. While we completely re-design the image and label encoding process, we append our TTS and TFC modules on top of the token matching module. Additionally, we append a small adapter module, LoRA [58], to the query and value features of attention mechanism in the image encoder, TFC and the token matching modules as shown in Fig. 1.

We strive to explore the effectiveness of *optimal diffusion time-step features* by applying to a universal few-shot dense prediction task, the first task introduced by VTM. We stress that we apply token matching after consolidating optimal diffusion features, similarly to VTM which likewise performs after encoding. Ours shows superiority over the ViT features when decoded in the same way as the VTM, demonstrating that diffusion models can perform competitively against the ViT-based architecture by only selecting adequate and optimal timestep features. Rather than substituting ViT with DM, we remark that we are the first to apply DMs to a few-shot dense prediction.

3.2 Task-aware Timestep Selection

Thanks for highlighting the importance of time-step selection.We presented a simple yet effective optimal time-step selection that allows for smooth gradient back-propagation, which may not be realizable with classical optimization algorithms. We design a Task-aware Timestep Selection, or TTS, module to select the most admissible timesteps from a sequence of timesteps spanning the entire diffusion decoder timesteps. In other words, our aim is to select k timesteps at which we extract timestep features from the decoder. Upon specifying the number of timestep features to select, k, and the initial set of k features, TTS module is to iteratively search for an optimal timestep feature set during training or task-specific fine-tuning, under the assumption that a pair of highly similar features may retain redundant visual information in terms of semantic or geometric details. Without loss of generality, our TTS module identifies the least synergic timestep feature to remove, and a newly sampled timestep feature has diverse enough information from that in the old set, thereby complementing each other in the subsequent consolidation stage.

As elaborated in Alg. 1 and illustrated in Fig. 2, TTS has two phases: finding the useless timestep from k features, and acquiring a new valuable timestep feature. Among the current set of timestep features, we assess which feature would potentially yield a negative effect when used together with the rest. To achieve this, we apply the Leave-One-Out selection strategy in which one timestep feature is held out at each time to compute the final task losses by forward passing with each held-out feature set of size $k-1$. We then remove the least informative timestep, t_r, corresponding to the held-out feature set with the highest task loss sum, formulated as follows:

$$t_r = \underset{t}{\operatorname{argmin}}\, \mathcal{L}_t, \quad \forall t \in \mathcal{T}_i = \{t_1, t_2, \cdots, t_k\}. \tag{2}$$

Given the eliminated feature set of size $k-1$, we sample a new timestep $t_{new} \sim U(1, t_{max})$. We then extract the corresponding timestep feature from the last block of the U-Net decoder at the sampled timestep, t_{new}, and compute pairwise feature similarity scores. Here, we further constrain the selection procedure by forcing the new timestep feature not to be too similar yet different (*i.e.,* similarity score $> \tau_{sim}$). Once the similarity constraint is met for all current feature set against the new timestep feature, we ensure that the task loss sum is lower than the running loss, similarly in the former phase. We repeat this procedure for N_{iter} number of iterations unless a new valid timestep feature is drawn into the updated feature set, $\mathcal{T}$.

3.3 Timestep Feature Consolidation

Given the updated timestep feature set, $\mathcal{T}$, we need to merge them in order to use as the key to the token matching and label decoder stage. Our Timestep Feature Consolidation (TFC) module closely follows the general cross attention mechanism [50,80]. As depicted in Fig. 2, we note that out TFC module matches the information between the support diffusion features and the support label features at the timestep channel via attention. Meanwhile, the token matching module (as well as in VTM) matches between the query image features and support image features–a key difference with our TFC module. Formally, we describe the consolidation procedure as follows:

$$\begin{aligned} k' &= \text{Softmax}\left(\frac{g(y_k^s)w_Q(f(x_k^s)w_K)^T}{\sqrt{d}}\right) \cdot f(x_k^s)w_V \\ &= O_{TS} \cdot f(x_k^s)w_V \end{aligned} \tag{3}$$

where the k' represents the new key vector for the attention of original matching module from Eq. 1 and $w_Q, w_K, w_V \in \mathbb{R}^{d\times d}$ are the weight matrix of query, key and value for the attention mechanism in TFC. The timestep attention matrix $O_{TS} \in \mathbb{R}^{T\times 1}$ shows the relationship between the diffusion features from multiple timesteps and label features for the target task. Therefore, examining this information encourages the original matching module to consider the characteristics of distinct diffusion timesteps for arbitrary dense prediction.

3.4 Parameter-efficient Fine-tuning

We further improve the performance of task-specific adaptation by adopting LoRA [58] as our adapter for few-shot dense prediction. LoRA is a recent yet already widely used method for adapting a pre-trained neural network to unseen target tasks under a small extra parameter budget. We deem that equipping LoRA to our model is suitable for dense prediction as it replaces the task-specific bias parameters during fine-tuning and avoids forgetting of trained task-agnostic knowledge after fine-tuning.

For a frozen U-Net [81] backbone weight matrix $W_0 \in \mathbb{R}^{d\times k}$, we attach low-rank matrices, B and A, to model the update $\Delta W \in \mathbb{R}^{d\times k}$ as BA as follows:

$$W_{fine-tuned} = W_0 + \Delta W = W_0 + BA, \tag{4}$$

where $B \in \mathbb{R}^{d \times r}$ and $A \in \mathbb{R}^{r \times k}$ with the bottleneck dimension $r \ll min(d, k)$. Following [58], we initialize A with uniform Kaiming distribution [82] and B with zero. We set the hyperpameters to $r = 2, \alpha = 4$ for adapters attached alongside the attention modules in the backbone and $r = 8, \alpha = 16$ for those in the rest, in order to minimize resources while maximizing capacity of the adapters. In addition, we add a dropout of 0.2 to inhibit overfitting to a particular task. This adapter is fine-tuned independently of the frozen weight matrices. To maximize the adaptation capacity at small computational footprints, we attach adapters to each of the attention modules in the backbone, our TFC module, and token matching module before the decoder, each at query and value as illustrated in Fig. 2. In terms of computational footprint, our fine-tuning adaptation requires approximately 305 KB (0.025% in proportion to total) in parameters, compared to 288 KB (0.28 %) in VTM [50]. In this regard, our adapter placement is lightweight, cost-effective, and competitive against the previous work.

4 Experiments

4.1 Implementation Details

Dataset. We evaluate our method on the *Tiny* subset (∼3.9 M instances) of Taskonomy dataset [83] to validate our few-shot learner on unseen dense prediction tasks. Taskonomy dataset is a large-scale dataset designed for multi-task learning containing indoor images and their annotations collected from 35 different buildings. The dataset spans 26+ tasks in total, from which we select ten benchmarked tasks including semantic segmentation (SS), surface normal (SN), Euclidean distance Depth (ED), Z-buffer Depth (ZD), Texture Edge (TE), Occlusion Edge (OE), 2D/3D Keypoints (K2/K3), Reshading (RS) and Principal Curvature (PC).

Following the first work [50] for a fair comparison, we construct these tasks into 5-fold splits such that each fold holds two related tasks for a few-shot evaluation, while cross-fold tasks remain sufficiently distinguished in task characteristics (i.e., K2/K3 tasks belong in the same fold and depth tasks (ED/ZD) are kept in a separate fold). For evaluation, we withhold one fold (*unseen* $\mathcal{D}_{test}$) and train on tasks ($\mathcal{D}_{train}$) in the remaining four folds. We augment task diversity in single-channel tasks (*e.g.,* ED, TE, OE) to multi-channels. All task labels are normalized to $[0, 1]$. During task-specific adaptation (finetuning), we randomly sample ten support sets from the train split. We refer to the *Supplementary Material* for details on pre-trained models and implementation details.

We point out that Taskonomy dataset (5-task) is widely used in multi-task learning (MTL) community [84, 85], along with NYUv2 (3-task) and Cityscapes (2-task). We extend the 5-task to a broader 10-task setting as practiced in VTM [50].We also highlight that Taskonomy is vastly different from mainstream perception datasets like COCO, which is geared toward image recognition tasks (detection, segmentation, and captioning), whereas Taskonomy is purposed for

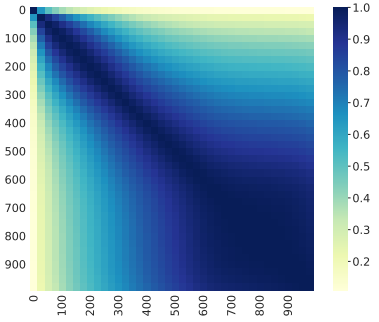

Fig. 3: Similarity scores for the timestep features from pre-trained SD v1.4.

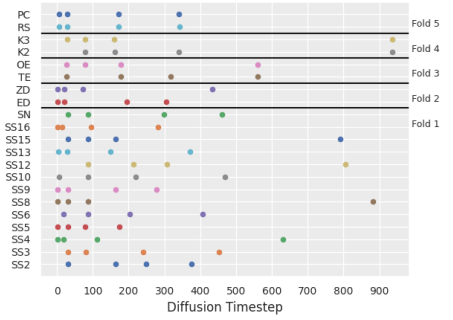

Fig. 4: Selected timesteps per task. For each task in the ordinate, the selected $k = 4$ timesteps are shown in the abscissa.

a *multitude of diverse* tasks (*e.g.,* depth, segmentation, curvature, edges and keypoints) paired with RGB.

Timestep selection. We conducted training using $k = 4$ timesteps due to hardware limitations. Motivated by [19], we set the initial timesteps to {1, 100, 200, 300} and performed the timestep search procedure with the feature similarity constraint with τ_{sim} set to 0.9, selected based on Fig. 3. This new timestep selection criterion not only refrains from selecting a new feature that is too similar to the old ones, but allows to maintain features of diverse semantic and geometric information that is present across all timesteps. Therefore, it is imperative to select this hyper-parameter in our design.

Evaluation Settings. Following [50], we compare our models with fully-supervised models and few-shot models on the Taskonomy-*Tiny* dataset. Few-shot models are trained and fine-tuned using the episodic meta-learning protocol while the fully-supervised models are trained without unseen tasks. For semantic segmentation (SS), we follow the common practice of segmentation protocol [86] and report the mean intersection over union (mIoU) across all classes. Continuous label tasks are evaluated using mean angle error (mErr) for surface normal prediction (SN) [87], and root mean square error (RMSE) for other tasks.

Baselines. For fair comparisons, we follow the baseline implementation details used int the VTM. Since HSNet [47], VAT [48], PGNet [88] is based on the convolutional layers, we use ResNet-101 backbone pre-trained for image classification on ImageNet-1K. For few-shot modification of HSNet, VAT, DPGNet, we follow the guidelines suggested by VTM which change the masking operation and channel operation to adopt the semantic segmentation model to general dense prediction model. For InvPT, DPT and VTM which is the Transformer-based model, we use the BEiT pre-trained on the ImageNet-22K.

Table 1: Quantitative evaluation on Taskonomy-*Tiny* dataset in full and few-shot ($N = 10$) supervision settings. † and ‡ denote uniform sampling in steps of 250 for $k = 4$, *i.e.*, $t_i \sim U((i-1) \cdot 1000/k, i \cdot 1000/k)$ for $i = [1, \cdots, k]$, and without fine-tuning adaptation, respectively. **Best** and second best for each fully supervised ("Full") and few-shot ("10-Shot") learning method groups.

Level of Supervision	Model	Taskonomy Tasks									
		Fold 1		Fold 2		Fold 3		Fold 4		Fold 5	
		SS	**SN**	**ED**	**ZD**	**TE**	**OE**	**K2**	**K3**	**RS**	**PC**
		mIoU ↑	mErr ↓	RMSE ↓	RMSE ↓	RMSE ↓	RMSE ↓	RMSE ↓	RMSE ↓	RMSE ↓	RMSE ↓
Full	DPT	**0.4449**	**6.4414**	**0.0534**	**0.0268**	**0.0188**	**0.0689**	**0.0358**	**0.0357**	**0.0860**	**0.0347**
	InvPT	0.3900	12.9249	0.0589	0.0298	0.0517	0.0788	0.0456	0.0384	0.0949	0.0370
10-Shot ($< 0.004\%$)	HSNet	0.1069	24.9120	0.2375	0.0748	0.1746	0.1643	0.1056	0.0651	0.2627	0.0610
	VAT	0.0353	25.8134	0.2718	0.0779	0.1719	0.1655	0.1450	0.0678	0.2709	0.0796
	DGPNet	0.0261	29.1668	0.4579	0.2846	0.1881	0.2130	0.1104	0.1308	0.3680	0.3574
	VTM (baseline)	0.4097	11.4391	0.0741	0.0316	**0.0791**	**0.0912**	**0.0639**	0.0519	**0.1089**	0.0420
	k Random $t \sim U(1, 1000)$	0.0942	21.0651	0.1232	0.0392	0.1153	0.1246	0.0978	0.0769	0.2299	0.0446
	k Stratified Random†	0.3506	11.3639	0.0881	0.0387	0.1067	0.1042	0.0801	0.0512	0.2311	0.0449
	Ours‡	0.0042	28.6767	0.1720	0.0659	0.1892	0.1896	0.1168	0.0530	0.2786	0.0623
	Ours	**0.4420**	**11.0004**	**0.0670**	**0.0306**	0.1032	0.0930	0.0740	**0.0496**	0.1125	**0.0412**

4.2 Experimental Results

Selected Timesteps. We visually depict the distribution of the selected timesteps used for testing in Fig. 4. For each task pair in each fold, the selected timesteps follow a similar distribution spread and range. We posit that this pattern is attributed to high task relevance and similar characteristics necessary for prediction such as semantic coherence, object boundary and geometry. Moreover, most tasks including semantic segmentation as widely known, exhibit stronger affinity to earlier timesteps. We conjecture that earlier timestep features contain the core semantics that benefit predictions in all tasks, while some tasks mutually benefit from several later ones.

Quantitative comparison. Table 1 displays the performance of our model across ten different tasks. With our successful design of TTS and TFC modules, we observe performance improvement in most tasks. Notably, semantic segmentation (SS) prediction achieves the highest gain in mIoU, almost on par with the fully supervised baseline results. On the other hand, we observe limited improvement in several tasks including TE, OE, K2 and RS. We attribute this weakness to the U-Net backbone structure, which insufficiently addresses the scale-sensitivity issue and understanding the spatial contexts in long ranges [89, 90]. Specifically, while diffusion features excel in 3D tasks with geometry (*e.g.,* SN, OE, K3, ZD, ED), they often fail in 2D tasks such as TE and K2 [91], partly due to training multiple tasks jointly.

Qualitative comparison. In Fig. 5, we present qualitative results of stratified random sampling (SRS) and our approach for all task folds. The results from SRS represent the straightforward lower quality on the all tasks and fail to learn the RS and PC. In the case of Semantic Segmentation task results, it is evident that our model predicts semantic details more clearly, while VTM often incorrectly predicts areas. When examining the results of surface normal or depth tasks with the VTM, our model predicts more accurate and clearer values in areas where

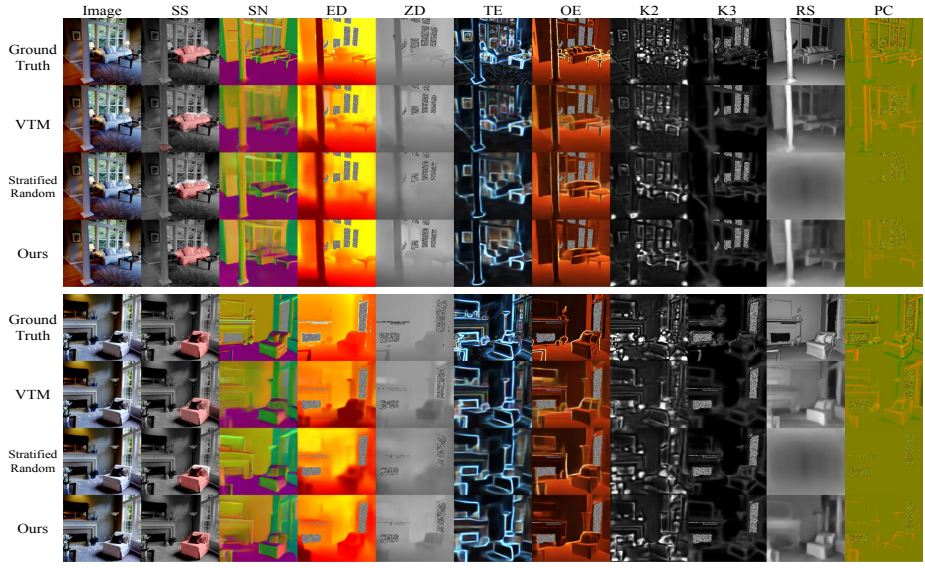

Fig. 5: Qualitative comparison. We visualize the qualitative results for all ten evaluated tasks in the Taskonomy-*Tiny* dataset. Ours (last row) mostly exhibits superior prediction results in all the experimented tasks.

objects exist. Overall, our model's results are comparable or of higher quality in prediction across various tasks.

Performance w/o adapter. In Table 1, we showed the performance when not using a fine-tuning adapter. We trained the model across four task folds and evaluated its performance on unseen tasks without fine-tuning. Due to the lack of information on unseen tasks, it was confirmed that performance was low across all tasks. This indicates the necessity of an effective adapter to predict unseen tasks.

Ablation study. To assess the effectiveness of our proposed modules, we conducted ablation studies on TTS and TFC as shown in Tables 2 and 3. Selecting a new timestep without the feature similarity constraint yielded performance degradation of 9.2% and 6.2% for SS and SN, respectively. Similarly, 0.5% and 4.5% performance loss in SS and SN tasks, respectively. While either module serves to effectively improve our few-shot performance, the cosine similarity threshold allows for more diverse features to be selected and the timestep-wise loss constraint encourages even more diversified timesteps in synergy. We also note that replacing TFC with summation or concatenation operation further degrades performance.

5 Discussion

We report the results for the classical random sampling methods in Table 1 and Fig. 5. While it is trivial to note that adaptive sampling is superior to random sampling approaches, we verify from the results that both random and stratified

Table 2: Ablation study on TTS.

Ablated Item	SS (mIoU ↑)	SN (mErr ↓)
w/o feature similiarity	0.4072	11.6790
w/o timestep-wise loss	0.4397	11.5043
Ours	**0.4420**	**11.0004**

Table 3: Ablation study on TFC.

Ablated Item	SS (mIoU ↑)	SN (mErr ↓)
Summation	0.4244	11.6858
Concatenation	0.4150	11.2220
Ours	**0.4420**	**11.0004**

Table 4: Performance comparison on fixed single and multiple timesteps (left), and adapter positions (right) with *Ours* on the tasks belonging to Fold 1.

Item	Single				Multiple	Ours		Adapter position
	0	250	500	750	0,250,500,750	Adaptive	UNet+TFC+Token matching	TFC+Token matching
SS (mIoU ↑)	0.4398	0.4224	0.1383	0.1260	0.4029	**0.4420**		0.4190
SN (mErr ↓)	11.5116	12.2057	19.4106	21.3307	13.1991	**11.0004**		11.1553

Table 5: Proportion of computations for our learnable TFC module.

Item	FLOPs (G)	Params (MB)
TFC module	60.587 (0.58%)	9.449 (0.91 %)
Total	10454	1036

random sampling fail to converge at ideal timesteps that benefit in all dense tasks of interest. A few surpassing occurrences for the stratified random sampling are attributed to purely chance events that would not consistently occur. Nonetheless, dividing the timestep range to multiple smaller strata does show intermittent advantages. In addition, we show in Table 4 that fixed timesteps do not necessarily result in better few-shot performance. While the earlier single timesteps are relatively better than the later ones since they are more semantically aware of objects [1, 18], manual combinations lead to unstable results due to negative transfer in timestep features.

Practical feasibility. Considering the practical desiderata of universal few-shot dense prediction, it is crucial to perform diffusion timestep selection and consolidation procedure at a relatively reduced computational burden. While the entire network consumes significant amount of computations and parameters by the inherent model architecture, we remark that our proposed learnable TFC module accounts for only 0.58 % and 0.91 % of total FLOPs and Parameter size, respectively. This entails a notable computational advantage when applying to other orthogonal diffusion model-based works.

Limitations. Our method has a few limitations in that we only divide range into strata based on similarity scores from Fig. 3, limiting generalizability. In addition, evaluation on the Taskonomy-*Tiny* subset may limit performance compared to *Medium* or *Full* subset.

6 Conclusion

In this paper, we closely examined and demonstrated the signifance of consolidating an optimal set of diffusion timesteps for universal few-shot learning of dense prediction tasks. Through meticulous exploration into adaptive timestep selection and motivation from earlier works on remarkable effectiveness of multiple

diverse diffusion timesteps on semantics- and geometry-focused tasks, we have proposed cost-effective task-oriented learnable timestep selection and consolidation method to fully leverage a pre-trained diffusion model to its full potential without the heuristic aspect. We remark that our proposed modules can be integrated into any diffusion model-based framework with one or more specified target task. Our project page with code will be hosted on Github.

References

1. J. Ho, A. Jain, and P. Abbeel, "Denoising diffusion probabilistic models," *Advances in neural information processing systems*, vol. 33, pp. 6840–6851, 2020. 1, 2, 3, 14
2. Y. Song, J. N. Sohl-Dickstein, D. P. Kingma, A. Kumar, S. Ermon, and B. Poole, "Score-based generative modeling through stochastic differential equations," *ArXiv*, vol. abs/2011.13456, 2020. 1
3. J. Song, C. Meng, and S. Ermon, "Denoising diffusion implicit models," *ArXiv*, vol. abs/2010.02502, 2020. 1, 3
4. R. Rombach, A. Blattmann, D. Lorenz, P. Esser, and B. Ommer, "High-resolution image synthesis with latent diffusion models," in *Proceedings of the IEEE/CVF conference on computer vision and pattern recognition*, pp. 10684–10695, 2022. 1, 3, 5, 7
5. Y. Ji, Z. Chen, E. Xie, L. Hong, X. Liu, Z. Liu, T. Lu, Z. Li, and P. Luo, "Ddp: Diffusion model for dense visual prediction," *arXiv preprint arXiv:2303.17559*, 2023. 1, 3
6. L. Li, H. Li, X. Zheng, J. Wu, X. Xiao, R. Wang, M. Zheng, X. Pan, F. Chao, and R. Ji, "Autodiffusion: Training-free optimization of time steps and architectures for automated diffusion model acceleration," in *Proceedings of the IEEE/CVF International Conference on Computer Vision*, pp. 7105–7114, 2023. 1, 3, 4
7. W. Peebles and S. Xie, "Scalable diffusion models with transformers," in *Proceedings of the IEEE/CVF International Conference on Computer Vision*, pp. 4195–4205, 2023. 1, 3
8. B. Kawar, M. Elad, S. Ermon, and J. Song, "Denoising diffusion restoration models," *Advances in Neural Information Processing Systems*, vol. 35, pp. 23593–23606, 2022. 1
9. H. Chung, B. Sim, and J. C. Ye, "Come-closer-diffuse-faster: Accelerating conditional diffusion models for inverse problems through stochastic contraction," in *Proceedings of the IEEE/CVF Conference on Computer Vision and Pattern Recognition*, pp. 12413–12422, 2022. 1
10. M. Daniels, T. Maunu, and P. Hand, "Score-based generative neural networks for large-scale optimal transport," *Advances in neural information processing systems*, vol. 34, pp. 12955–12965, 2021. 1
11. C. Saharia, J. Ho, W. Chan, T. Salimans, D. J. Fleet, and M. Norouzi, "Image super-resolution via iterative refinement," *IEEE Transactions on Pattern Analysis and Machine Intelligence*, vol. 45, pp. 4713–4726, 2021. 1
12. J. Whang, M. Delbracio, H. Talebi, C. Saharia, A. G. Dimakis, and P. Milanfar, "Deblurring via stochastic refinement," *2022 IEEE/CVF Conference on Computer Vision and Pattern Recognition (CVPR)*, pp. 16272–16282, 2021. 1
13. T. Amit, T. Shaharbany, E. Nachmani, and L. Wolf, "Segdiff: Image segmentation with diffusion probabilistic models," *arXiv preprint arXiv:2112.00390*, 2021. 1

14. J. Wolleb, R. Sandkühler, F. Bieder, P. Valmaggia, and P. C. Cattin, "Diffusion models for implicit image segmentation ensembles," in *International Conference on Medical Imaging with Deep Learning*, pp. 1336–1348, PMLR, 2022. 1
15. D. Baranchuk, I. Rubachev, A. Voynov, V. Khrulkov, and A. Babenko, "Label-efficient semantic segmentation with diffusion models," *arXiv preprint arXiv:2112.03126*, 2021. 1
16. J. Wu, H. Fang, Y. Zhang, Y. Yang, and Y. Xu, "Medsegdiff: Medical image segmentation with diffusion probabilistic model," *ArXiv*, vol. abs/2211.00611, 2022. 1
17. Y. Xie and Q. Li, "Measurement-conditioned denoising diffusion probabilistic model for under-sampled medical image reconstruction," in *International Conference on Medical Image Computing and Computer-Assisted Intervention*, 2022. 1
18. J. Choi, J. Lee, C. Shin, S. Kim, H. J. Kim, and S.-H. Yoon, "Perception prioritized training of diffusion models," *2022 IEEE/CVF Conference on Computer Vision and Pattern Recognition (CVPR)*, pp. 11462–11471, 2022. 2, 14
19. D. Baranchuk, I. Rubachev, A. Voynov, V. Khrulkov, and A. Babenko, "Label-efficient semantic segmentation with diffusion models," *ArXiv*, vol. abs/2112.03126, 2021. 2, 3, 4, 11
20. O. Ronneberger, P. Fischer, and T. Brox, "U-net: Convolutional networks for biomedical image segmentation," *ArXiv*, vol. abs/1505.04597, 2015. 2
21. G. Luo, L. Dunlap, D. H. Park, A. Holynski, and T. Darrell, "Diffusion hyperfeatures: Searching through time and space for semantic correspondence," *arXiv preprint arXiv:2305.14334*, 2023. 2, 4
22. J. Song, C. Meng, and S. Ermon, "Denoising diffusion implicit models," *arXiv:2010.02502*, October 2020. 3
23. Y. Song, J. Sohl-Dickstein, D. P. Kingma, A. Kumar, S. Ermon, and B. Poole, "Score-based generative modeling through stochastic differential equations," in *International Conference on Learning Representations*, 2021. 3
24. P. Dhariwal and A. Nichol, "Diffusion models beat gans on image synthesis," *Advances in neural information processing systems*, vol. 34, pp. 8780–8794, 2021. 3
25. I. J. Goodfellow, J. Pouget-Abadie, M. Mirza, B. Xu, D. Warde-Farley, S. Ozair, A. C. Courville, and Y. Bengio, "Generative adversarial nets," in *NIPS*, 2014. 3
26. A. Radford, J. W. Kim, C. Hallacy, A. Ramesh, G. Goh, S. Agarwal, G. Sastry, A. Askell, P. Mishkin, J. Clark, *et al.*, "Learning transferable visual models from natural language supervision," in *International conference on machine learning*, pp. 8748–8763, PMLR, 2021. 3
27. X. Yang and X. Wang, "Diffusion model as representation learner," in *Proceedings of the IEEE/CVF International Conference on Computer Vision*, pp. 18938–18949, 2023. 3
28. E. Hedlin, G. Sharma, S. Mahajan, H. Isack, A. Kar, A. Tagliasacchi, and K. M. Yi, "Unsupervised semantic correspondence using stable diffusion," *Advances in Neural Information Processing Systems*, vol. 36, 2024. 3
29. Z. Li, Q. Zhou, X. Zhang, Y. Zhang, Y. Wang, and W. Xie, "Guiding text-to-image diffusion model towards grounded generation," *arXiv preprint arXiv:2301.05221*, 2023. 3
30. W. Zhao, Y. Rao, Z. Liu, B. Liu, J. Zhou, and J. Lu, "Unleashing text-to-image diffusion models for visual perception," *ArXiv*, vol. abs/2303.02153, 2023. 3
31. J. Xu, S. Liu, A. Vahdat, W. Byeon, X. Wang, and S. De Mello, "Open-vocabulary panoptic segmentation with text-to-image diffusion models," in *Proceedings of the IEEE/CVF Conference on Computer Vision and Pattern Recognition*, pp. 2955–2966, 2023. 3

32. Z. Li, Q. Zhou, X. Zhang, Y. Zhang, Y. Wang, and W. Xie, "Open-vocabulary object segmentation with diffusion models," 2023. 3
33. J. Wynn and D. Turmukhambetov, "DiffusioNeRF: Regularizing Neural Radiance Fields with Denoising Diffusion Models," in *CVPR*, 2023. 3
34. B. Poole, A. Jain, J. T. Barron, and B. Mildenhall, "Dreamfusion: Text-to-3d using 2d diffusion," *arXiv*, 2022. 3
35. J. Zhou, J. Sheng, J. Fan, P. Ye, T. He, B. Wang, and T. Chen, "When hyperspectral image classification meets diffusion models: An unsupervised feature learning framework," *arXiv preprint arXiv:2306.08964*, 2023. 4
36. J. Xu, S. Liu, A. Vahdat, W. Byeon, X. Wang, and S. D. Mello, "Open-vocabulary panoptic segmentation with text-to-image diffusion models," *2023 IEEE/CVF Conference on Computer Vision and Pattern Recognition (CVPR)*, pp. 2955–2966, 2023. 4
37. B. Kang, Z. Liu, X. Wang, F. Yu, J. Feng, and T. Darrell, "Few-shot object detection via feature reweighting," in *Proceedings of the IEEE/CVF International Conference on Computer Vision*, pp. 8420–8429, 2019. 4
38. X. Wang, T. Huang, T. Darrell, J. Gonzalez, and F. Yu, "Frustratingly simple few-shot object detection. arxiv 2020," *arXiv preprint arXiv:2003.06957*. 4
39. J. Wu, S. Liu, D. Huang, and Y. Wang, "Multi-scale positive sample refinement for few-shot object detection," in *Computer Vision–ECCV 2020: 16th European Conference, Glasgow, UK, August 23–28, 2020, Proceedings, Part XVI 16*, pp. 456–472, Springer, 2020. 4
40. C. Li, H. Liu, L. Li, P. Zhang, J. Aneja, J. Yang, P. Jin, H. Hu, Z. Liu, Y. J. Lee, *et al.*, "Elevater: A benchmark and toolkit for evaluating language-augmented visual models," *Advances in Neural Information Processing Systems*, vol. 35, pp. 9287–9301, 2022. 4
41. K. Wang, J. H. Liew, Y. Zou, D. Zhou, and J. Feng, "Panet: Few-shot image semantic segmentation with prototype alignment," in *proceedings of the IEEE/CVF international conference on computer vision*, pp. 9197–9206, 2019. 4
42. C. Ouyang, C. Biffi, C. Chen, T. Kart, H. Qiu, and D. Rueckert, "Self-supervision with superpixels: Training few-shot medical image segmentation without annotation," in *Computer Vision–ECCV 2020: 16th European Conference, Glasgow, UK, August 23–28, 2020, Proceedings, Part XXIX 16*, pp. 762–780, Springer, 2020. 4
43. Z. Tian, H. Zhao, M. Shu, Z. Yang, R. Li, and J. Jia, "Prior guided feature enrichment network for few-shot segmentation," *IEEE transactions on pattern analysis and machine intelligence*, vol. 44, no. 2, pp. 1050–1065, 2020. 4
44. Y. Liu, X. Zhang, S. Zhang, and X. He, "Part-aware prototype network for few-shot semantic segmentation," in *Computer Vision–ECCV 2020: 16th European Conference, Glasgow, UK, August 23–28, 2020, Proceedings, Part IX 16*, pp. 142–158, Springer, 2020. 4
45. Z. Fan, J.-G. Yu, Z. Liang, J. Ou, C. Gao, G.-S. Xia, and Y. Li, "Fgn: Fully guided network for few-shot instance segmentation," in *Proceedings of the IEEE/CVF conference on computer vision and pattern recognition*, pp. 9172–9181, 2020. 4
46. D. A. Ganea, B. Boom, and R. Poppe, "Incremental few-shot instance segmentation," in *Proceedings of the IEEE/CVF Conference on Computer Vision and Pattern Recognition*, pp. 1185–1194, 2021. 4
47. J. Min, D. Kang, and M. Cho, "Hypercorrelation squeeze for few-shot segmentation," in *Proceedings of the IEEE/CVF International Conference on Computer Vision (ICCV)*, 2021. 4, 11

48. S. Hong, S. Cho, J. Nam, S. Lin, and S. Kim, "Cost aggregation with 4d convolutional swin transformer for few-shot segmentation," in *European Conference on Computer Vision*, pp. 108–126, Springer, 2022. 4, 11
49. J. Johnander, J. Edstedt, M. Felsberg, F. S. Khan, and M. Danelljan, "Dense gaussian processes for few-shot segmentation," in *European Conference on Computer Vision*, 2021. 4
50. D. Kim, J. Kim, S. Cho, C. Luo, and S. Hong, "Universal few-shot learning of dense prediction tasks with visual token matching," *arXiv preprint arXiv:2303.14969*, 2023. 4, 5, 6, 7, 9, 10, 11
51. O. Vinyals, C. Blundell, T. Lillicrap, D. Wierstra, *et al.*, "Matching networks for one shot learning," *Advances in neural information processing systems*, vol. 29, 2016. 4, 6
52. T. Dettmers, A. Pagnoni, A. Holtzman, and L. Zettlemoyer, "Qlora: Efficient finetuning of quantized llms," *Advances in Neural Information Processing Systems*, vol. 36, 2024. 4
53. S.-Y. Liu, C.-Y. Wang, H. Yin, P. Molchanov, Y.-C. F. Wang, K.-T. Cheng, and M.-H. Chen, "Dora: Weight-decomposed low-rank adaptation," *arXiv preprint arXiv:2402.09353*, 2024. 4
54. Y.-L. Sung, J. Cho, and M. Bansal, "Vl-adapter: Parameter-efficient transfer learning for vision-and-language tasks," in *Proceedings of the IEEE/CVF Conference on Computer Vision and Pattern Recognition*, pp. 5227–5237, 2022. 4
55. Y. Qiao, Z. Yu, and Q. Wu, "Vln-petl: Parameter-efficient transfer learning for vision-and-language navigation," in *Proceedings of the IEEE/CVF International Conference on Computer Vision*, pp. 15443–15452, 2023. 4
56. N. Houlsby, A. Giurgiu, S. Jastrzebski, B. Morrone, Q. De Laroussilhe, A. Gesmundo, M. Attariyan, and S. Gelly, "Parameter-efficient transfer learning for nlp," in *International Conference on Machine Learning*, pp. 2790–2799, PMLR, 2019. 5, 7
57. H. Liu, D. Tam, M. Muqeeth, J. Mohta, T. Huang, M. Bansal, and C. A. Raffel, "Few-shot parameter-efficient fine-tuning is better and cheaper than in-context learning," *Advances in Neural Information Processing Systems*, vol. 35, pp. 1950–1965, 2022. 5
58. E. J. Hu, Y. Shen, P. Wallis, Z. Allen-Zhu, Y. Li, S. Wang, L. Wang, and W. Chen, "Lora: Low-rank adaptation of large language models," *arXiv preprint arXiv:2106.09685*, 2021. 5, 8, 9, 10
59. A. Edalati, M. Tahaei, I. Kobyzev, V. P. Nia, J. J. Clark, and M. Rezagholizadeh, "Krona: Parameter efficient tuning with kronecker adapter," *arXiv preprint arXiv:2212.10650*, 2022. 5
60. M. Valipour, M. Rezagholizadeh, I. Kobyzev, and A. Ghodsi, "Dylora: Parameter efficient tuning of pre-trained models using dynamic search-free low-rank adaptation," *arXiv preprint arXiv:2210.07558*, 2022. 5
61. Q. Zhang, M. Chen, A. Bukharin, P. He, Y. Cheng, W. Chen, and T. Zhao, "Adaptive budget allocation for parameter-efficient fine-tuning," *arXiv preprint arXiv:2303.10512*, 2023. 5
62. F. Zhang, L. Li, J. Chen, Z. Jiang, B. Wang, and Y. Qian, "Increlora: Incremental parameter allocation method for parameter-efficient fine-tuning," *arXiv preprint arXiv:2308.12043*, 2023. 5
63. L. Zhang, L. Zhang, S. Shi, X. Chu, and B. Li, "Lora-fa: Memory-efficient low-rank adaptation for large language models fine-tuning," *arXiv preprint arXiv:2308.03303*, 2023. 5

64. B. Zi, X. Qi, L. Wang, J. Wang, K.-F. Wong, and L. Zhang, "Delta-lora: Fine-tuning high-rank parameters with the delta of low-rank matrices," *arXiv preprint arXiv:2309.02411*, 2023. 5
65. M. Zhang, C. Shen, Z. Yang, L. Ou, X. Yu, B. Zhuang, *et al.*, "Pruning meets low-rank parameter-efficient fine-tuning," *arXiv preprint arXiv:2305.18403*, 2023. 5
66. A. Tang, L. Shen, Y. Luo, Y. Zhan, H. Hu, B. Du, Y. Chen, and D. Tao, "Parameter efficient multi-task model fusion with partial linearization," *arXiv preprint arXiv:2310.04742*, 2023. 5
67. Q. Liu, X. Wu, X. Zhao, Y. Zhu, D. Xu, F. Tian, and Y. Zheng, "Moelora: An moe-based parameter efficient fine-tuning method for multi-task medical applications," *arXiv preprint arXiv:2310.18339*, 2023. 5
68. S. Luo, Y. Tan, S. Patil, D. Gu, P. von Platen, A. Passos, L. Huang, J. Li, and H. Zhao, "Lcm-lora: A universal stable-diffusion acceleration module," *arXiv preprint arXiv:2311.05556*, 2023. 5
69. R. Gandikota, J. Materzynska, T. Zhou, A. Torralba, and D. Bau, "Concept sliders: Lora adaptors for precise control in diffusion models," *arXiv preprint arXiv:2311.12092*, 2023. 5
70. L. Caccia, E. Ponti, Z. Su, M. Pereira, N. Le Roux, and A. Sordoni, "Multi-head adapter routing for cross-task generalization," in *Thirty-seventh Conference on Neural Information Processing Systems*, 2023. 5
71. R. Ranftl, K. Lasinger, D. Hafner, K. Schindler, and V. Koltun, "Towards robust monocular depth estimation: Mixing datasets for zero-shot cross-dataset transfer," *IEEE Transactions on Pattern Analysis and Machine Intelligence (TPAMI)*, 2020. 5, 6, 8
72. J. Deng, W. Dong, R. Socher, L.-J. Li, K. Li, and L. Fei-Fei, "Imagenet: A large-scale hierarchical image database," in *2009 IEEE Conference on Computer Vision and Pattern Recognition*, pp. 248–255, 2009. 6
73. H. Bao, L. Dong, S. Piao, and F. Wei, "Beit: Bert pre-training of image transformers," *arXiv preprint arXiv:2106.08254*, 2021. 6
74. E. Ben Zaken, Y. Goldberg, and S. Ravfogel, "BitFit: Simple parameter-efficient fine-tuning for transformer-based masked language-models," in *Proceedings of the 60th Annual Meeting of the Association for Computational Linguistics (Volume 2: Short Papers)* (S. Muresan, P. Nakov, and A. Villavicencio, eds.), (Dublin, Ireland), pp. 1–9, Association for Computational Linguistics, May 2022. 7
75. B. Lester, R. Al-Rfou, and N. Constant, "The power of scale for parameter-efficient prompt tuning," in *Proceedings of the 2021 Conference on Empirical Methods in Natural Language Processing* (M.-F. Moens, X. Huang, L. Specia, and S. W.-t. Yih, eds.), (Online and Punta Cana, Dominican Republic), pp. 3045–3059, Association for Computational Linguistics, Nov. 2021. 7
76. Y. Li, S. Xie, X. Chen, P. Dollar, K. He, and R. Girshick, "Benchmarking detection transfer learning with vision transformers," *arXiv preprint arXiv:2111.11429*, 2021. 7
77. M. Jia, L. Tang, B.-C. Chen, C. Cardie, S. Belongie, B. Hariharan, and S.-N. Lim, "Visual prompt tuning," in *European Conference on Computer Vision*, pp. 709–727, Springer, 2022. 7
78. Z. Chen, Y. Duan, W. Wang, J. He, T. Lu, J. Dai, and Y. Qiao, "Vision transformer adapter for dense predictions," *arXiv preprint arXiv:2205.08534*, 2022. 7
79. C. Schuhmann, R. Beaumont, R. Vencu, C. Gordon, R. Wightman, M. Cherti, T. Coombes, A. Katta, C. Mullis, M. Wortsman, *et al.*, "Laion-5b: An open large-

scale dataset for training next generation image-text models," *Advances in Neural Information Processing Systems*, vol. 35, pp. 25278–25294, 2022. 7
80. C.-F. R. Chen, Q. Fan, and R. Panda, "Crossvit: Cross-attention multi-scale vision transformer for image classification," in *Proceedings of the IEEE/CVF international conference on computer vision*, pp. 357–366, 2021. 9
81. O. Ronneberger, P. Fischer, and T. Brox, "U-net: Convolutional networks for biomedical image segmentation," in *Medical Image Computing and Computer-Assisted Intervention–MICCAI 2015: 18th International Conference, Munich, Germany, October 5-9, 2015, Proceedings, Part III 18*, pp. 234–241, Springer, 2015. 9
82. K. He, X. Zhang, S. Ren, and J. Sun, "Deep residual learning for image recognition," in *Proceedings of the IEEE conference on computer vision and pattern recognition*, pp. 770–778, 2016. 10
83. A. R. Zamir, A. Sax, W. Shen, L. J. Guibas, J. Malik, and S. Savarese, "Taskonomy: Disentangling task transfer learning," in *Proceedings of the IEEE conference on computer vision and pattern recognition*, pp. 3712–3722, 2018. 10
84. L. Zhang, X. Liu, and H. Guan, "Automtl: A programming framework for automating efficient multi-task learning," in *Advances in Neural Information Processing Systems* (S. Koyejo, S. Mohamed, A. Agarwal, D. Belgrave, K. Cho, and A. Oh, eds.), vol. 35, pp. 34216–34228, Curran Associates, Inc., 2022. 10
85. X. Sun, R. Panda, R. Feris, and K. Saenko, "Adashare: Learning what to share for efficient deep multi-task learning," *Advances in Neural Information Processing Systems*, vol. 33, pp. 8728–8740, 2020. 10
86. A. Shaban, S. Bansal, Z. Liu, I. Essa, and B. Boots, "One-shot learning for semantic segmentation," *ArXiv*, vol. abs/1709.03410, 2017. 11
87. D. Eigen and R. Fergus, "Predicting depth, surface normals and semantic labels with a common multi-scale convolutional architecture," *2015 IEEE International Conference on Computer Vision (ICCV)*, pp. 2650–2658, 2014. 11
88. J. Johnander, J. Edstedt, M. Felsberg, F. S. Khan, and M. Danelljan, "Dense gaussian processes for few-shot segmentation," in *European Conference on Computer Vision*, pp. 217–234, Springer, 2022. 11
89. S. He, R. Bao, P. E. Grant, and Y. Ou, "U-netmer: U-net meets transformer for medical image segmentation," *arXiv preprint arXiv:2304.01401*, 2023. 12
90. H. Sahli, A. B. Slama, and M. Sayadi, "Skin lesion segmentation based on modified u-net architecture," in *2023 IEEE International Conference on Advanced Systems and Emergent Technologies (IC_ASET)*, pp. 1–5, IEEE, 2023. 12
91. A. Achille, M. Lam, R. Tewari, A. Ravichandran, S. Maji, C. C. Fowlkes, S. Soatto, and P. Perona, "Task2vec: Task embedding for meta-learning," in *Proceedings of the IEEE/CVF International Conference on Computer Vision (ICCV)*, October 2019. 12